AIP | Journal of Applied Physics

The magnetocaloric effect and critical behavior in amorphous Gd60Co40−xMnx alloys

Z. G. Zheng, X. C. Zhong, H. Y. Yu, V. Franco, Z. W. Liu, and D. C. Zeng

Citation: Journal of Applied Physics **111**, 07A922 (2012); doi: 10.1063/1.3673860
View online: http://dx.doi.org/10.1063/1.3673860
View Table of Contents: http://scitation.aip.org/content/aip/journal/jap/111/7?ver=pdfcov
Published by the AIP Publishing

The magnetocaloric effect and critical behavior in amorphous $Gd_{60}Co_{40-x}Mn_x$ alloys

Z. G. Zheng,[1] X. C. Zhong,[1] H. Y. Yu,[1] V. Franco,[2] Z. W. Liu,[1,a)] and D. C. Zeng[1,a)]
[1]*School of Materials Science & Engineering, South China University of Technology, Guangzhou 510640, People's Republic of China*
[2]*Department of Condensed Matter Physics, ICMSE-CSIC, Sevilla University, P.O. Box 1065, 41080 Sevilla, Spain*

(Presented 31 October 2011; received 23 September 2011; accepted 1 November 2011; published online 29 February 2012)

The amorphous alloys $Gd_{60}Co_{40-x}Mn_x$ (x = 0, 5, 10, 15) were prepared by melt spinning. The Curie temperature, T_c, increases monotonously with Mn addition, ranging from 198 K for x = 0 to 205 K for x = 15, while the maximum values of $-\Delta S_M$ under the applied field change from 0 to 5 T are 7.7, 7.1, 6.2 and 5.4 $J \cdot kg^{-1} \cdot K^{-1}$ for x = 0, 5, 10, and 15, respectively. All samples undergo a second order ferri-paramagnetic phase transition. The critical behavior around the transition temperature is investigated in detail, using both the standard Kouvel-Fisher procedure as well as the study of the field dependence of the magnetocaloric effect. Results indicate that the obtained critical exponents are reliable, and that the present alloys exhibit local magnetic interaction. © *2012 American Institute of Physics*. [doi:10.1063/1.3673860]

The magnetic materials with large magnetocaloric effect (MCE) have attracted considerable attention for magnetic refrigeration applications. In recent years, MCE has been found in various intermetallic alloys, such as $Gd_5Si_2Ge_2$,[1] $La(Fe,Si)_{13}$,[2,3] $MnAs_{1-x}Sb_x$,[4] $MnFeP_{1-x}Si_x$,[5] Ni-Mn-In,[6] and amorphous alloys $Fe_{88-2x}Co_xNi_xZr_7B_4Cu_1$.[7] However, a material with a large ΔS_m does not necessarily have a large refrigeration efficiency. The refrigerant capacity (RC) can provide an estimate of the performance of a magnetocaloric material.[8]

Recently, Gd based soft magnetic amorphous alloys, a type of second order phase transition (SOT) materials, have been proposed as the promising candidates for magnetic refrigerant. Owing to the amorphous nature, they exhibit some special advantages such as the negligible magnetic hysteresis loss, higher electrical resistivity, tunable Curie temperature T_c, high corrosion resistance, and large refrigerant capacity. Zhong *et al.*[9] found that amorphous $Gd_{68-x}Ni_{32+x}$ have large refrigerant capacity (RC) and the maximum RC value is 724 $J \cdot kg^{-1}$ with $\Delta H = 5$ T. For $Gd_{71}Co_{29}$ amorphous alloys,[10] the magnetic entropy changes ΔS_M under a magnetic field of 10 kOe is $-3.1\ J \cdot kg^{-1}\ K^{-1}$. Fu *et al.*[11] investigated the magnetic bulk metallic glass $Gd_{52.5}Co_{16.5}Al_{31}$, which has T_c of 95 K and $-\Delta S_{max}$ of 9.8 $J \cdot kg^{-1}\ K^{-1}$ under a field change of 5 T.

In this work, the effects of Mn on magnetic and magnetocaloric properties of $Gd_{60}Co_{40-x}Mn_x$ alloys are investigated. To investigate the nature of the ferrimagnetic (FM) to paramagnetic (PM) phase transition, we also performed a critical exponent study using the isothermal magnetization data around T_c.

The $Gd_{60}Co_{40-x}Mn_x$ (x = 0, 5, 10, 15) alloy buttons were prepared by arc-melting a mixture of pure Gd (99.95 wt%), Co (99.9 wt%) and Mn (99.5 wt%) in an argon atmosphere. To ensure composition homogeneity, the ingots were repeatedly melted at least four times. The crashed pieces of ingot were then melt-spun into ribbons (with a thickness of about 20–30 μm and a width of 3 mm) on a copper wheel with a speed of 50 m/s using a single-roller melt-spinner in an argon atmosphere. The microstructure of the alloys was characterized by a Philips X'pert Pro MPD X diffractometer, using a monochromatized X-ray beam with nickel filtered Cu Kα radiation (1.54056 Å). The temperature and magnetic field dependences of magnetization were measured by a Physical Properties Measurement System (PPMS-9, Quantum Design Co.).

For the X-ray diffraction patterns of all ribbon samples (not shown here), only one broad peak appears between 2θ of 30 and 40 degrees in all alloys, and no obvious diffraction peaks corresponding to crystalline phase are observed, indicating an amorphous structure in the $Gd_{60}Co_{40-x}Mn_x$ ternary alloys. For x = 0, there is a small peak near $2\theta = 28°$, indicating that it may be caused by some nanocrystal Gd.

Figure 1 presents the magnetization as a function of temperature for $Gd_{60}Co_{40-x}Mn_x$ amorphous alloys from 5 to 300 K under an applied field of 500 Oe. With the increase of temperature, the magnetization decreases, resulting from the magnetic transition from FM ordered state to PM ordered state. The Curie temperatures, T_c, determined as the temperature at the maximum of $|dM/dT|$ versus T plot shown in the insert, are 198 K, 202 K, 204 K and 205 K for x = 0, x = 5, x = 10 and x = 15, respectively.

The magnetocaloric effects of the series of alloys was calculated in terms of isothermal magnetic entropy change using Maxwell's equation. Figure 2 shows the temperature dependency of $-\Delta S_M$ under the applied magnetic field changes of 2 T and 5 T. The peak values of $-\Delta S_M$ are found to be 7.7, 7.1, 6.2 and 5.4 $J \cdot kg^{-1} \cdot K^{-1}$ for x = 0, 5, 10, and 15 respectively. These values are comparable to or even higher than those of $Gd_{65}Fe_{20}Al_8B_7$ amorphous alloy (5.21 $J \cdot kg^{-1} \cdot K^{-1}$ at 5 T)[12] and $Gd_{60}Al_{10}Mn_{30}$ nanocomposite (3.3 $J \cdot kg^{-1} \cdot K^{-1}$ at 5 T).[13]

The Arrott plots of the $Gd_{60}Co_{40-x}Mn_x$ (x = 5) amorphous ribbons are displayed in Fig. 3. The isothermal magnetization M-H curves are presented in the inset. A typical ferrimagnetic

a)Authors to whom correspondence should be addressed. Electronic addresses: zwliu@scut.edu.cn and medczeng@scut.edu.cn.

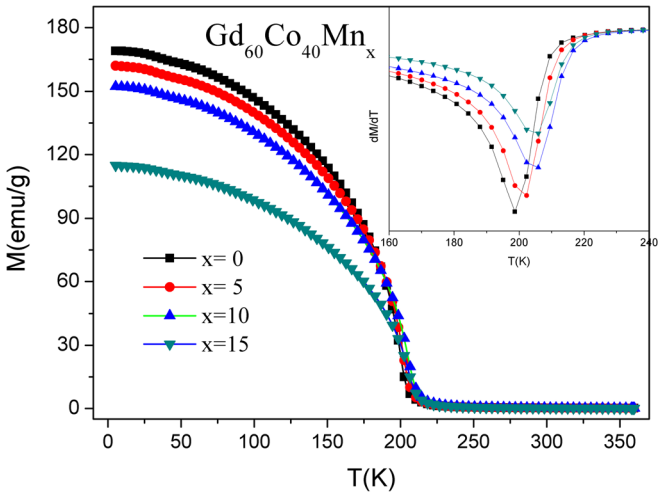

FIG. 1. (Color online) Temperature dependences of magnetization for $Gd_{60}Co_{40-x}Mn_x$ amorphous alloys under an applied field of 500 Oe.

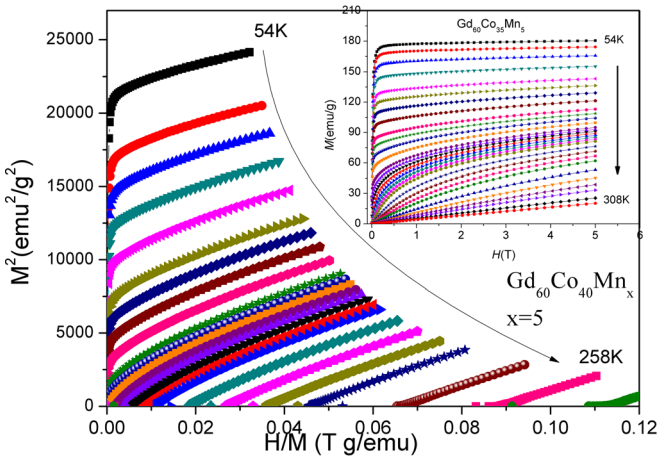

FIG. 3. (Color online) The Arrott plots of $Gd_{60}Co_{40-x}Mn_x$ (x = 5) amorphous alloy. The insert is isothermal magnetization curves as a function of magnetic field.

transition is evident in the vicinity of T_c. From Fig. 3, no inflection or negative slope is observed as an indication that FM – PM transition is of second-order.[12,14] Similar behavior has also been found for the whole series of alloys studied in this work.

The second-order transition from FM to PM near the Curie point is characterized by a set of critical exponents: β (associated with the spontaneous magnetization), γ (relevant to the initial susceptibility), and δ (associated with the critical magnetization isotherm). They are defined as:[15]

$$M_s(0,T) = m_0|t|^{\beta}, \quad t \le 0 \tag{1}$$

$$\chi_0^{-1}(0,T) = \frac{h_0}{m_0}|t|^{\gamma}, \quad t \ge 0 \tag{2}$$

$$H = DM^{\delta}, \quad t = 0 \tag{3}$$

where t is the reduced temperature ($t = T/T_c - 1$), and m_0, h_0 and D are the critical amplitudes. $M_s(0, T)$ is the spontaneous magnetization at different temperatures; χ_0^{-1} is the inverse of the susceptibility. Although the different critical exponents can be determined independently from experimental measurements, they are related to each other, which is taken in most cases to be of the form $\beta + \gamma = \beta\delta$. In order to properly determine the T_c, as well as the critical exponents β, γ, and δ, several methods can be used, including modified Arrott plots technique (MAPs), Kouvel–Fisher (KF) method and Widom scaling relation.[16] More recently, it has been shown that the field dependence of the magnetocaloric effect can be used to determine the critical exponents of materials.[17,18]

For the Kouvel–Fisher method, two additional magnitudes are defined as:

$$Y(T) = -M_s\left(\frac{\partial M_s}{\partial T}\right)^{-1} = -\frac{T - T_c}{\beta} \tag{4}$$

$$X(T) = \chi^{-1}\left(\frac{\partial \chi^{-1}}{\partial T}\right)^{-1} = \frac{T - T_c}{\gamma} \tag{5}$$

By plotting Y(T) and X(T) as a function of temperature, one should get straight lines around T_c with the slopes of $-1/\beta$ and $1/\gamma$, respectively, and the intercepts on the temperature axes are equal to T_c.

The exponents obtained from KF method are as follows: $\beta = 0.311$, $\gamma = 1.306$ with $T_c = 203.9$ K. All these critical exponents derived from various methods, including the KF method and scaling of the magnetocaloric effect, are given in Table I along with the theoretically predicted values for different models, such as Mean-field theory, three-dimensional (3D) Heisenberg theory and three-dimensional (3D) Ising theory. It should be noted that the 3D Heisenberg model or 3D Ising model is based on the short-range magnetic coupling, and mean-field theory is based on the long-range magnetic coupling. The magnetic interactions in the present alloys exhibit local magnetic interactions. It is clear from Table I that, with increasing Mn contents, the values of critical exponent β and γ increase continuously. Physically, β describes how the ordered moment grows below T_c while γ describes the divergence of the magnetic susceptibility at T_c. The smaller the value of β, the faster the growth of the ordered moment. The β value increases with increasing Mn contents, reflecting a slower growth of the ordered moment with decreasing temperature. This tendency is in agreement with magnetization intensity below T_c, which decreases with increasing Mn contents, as shown in the Fig. 1. Also, the

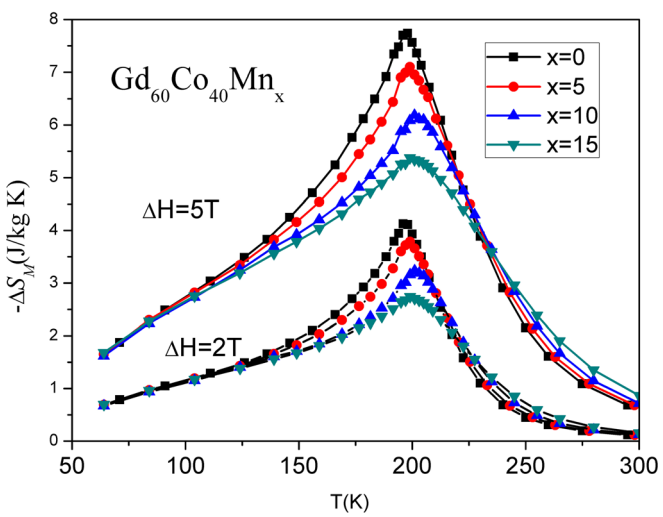

FIG. 2. (Color online) Magnetic entropy changes in the $Gd_{60}Co_{40-x}Mn_x$ amorphous ribbons under the magnetic field changes of 2 T and 5 T.

TABLE I. The values of the exponents β, γ, and δ as determined from Kouvel−Fisher method for $Gd_{60}Co_{40-x}Mn_x$. The theoretically predicted values of exponents for various universal classes are also given for the sake of comparison.

Composition	β	γ	δ	Reference
x = 0	0.309[0.308]	1.252[1.417]	5.051[a][5.601]	This work
x = 5	0.311[0.315]	1.306[1.733]	5.120[a][6.502]	This work
x = 10	0.322[0.328]	1.362[1.872]	5.229[a][6.707]	This work
x = 15	0.326[0.329]	1.580[1.954]	5.846[a][6.940]	This work
Mean-field theory	0.5	1.0	3.0	20–22
3D Heisenberg theory	0.365	1.336	4.8	20–22
3D Ising theory	0.325	1.24	4.82	20–22

[a]The values calculated using the relation $\beta + \gamma = \beta\delta$. Values without brackets are calculated using the Kouvel-Fisher method; square brackets indicate that the calculation is done using the scaling of the magnetocaloric effect.

change in the values of critical exponents is due to the formation of finite magnetic clusters in the infinite ferromagnetic network.[19]

In terms of renormalized magnetization $m = \frac{M}{|t|^{\beta}}$ and renormalized field $h = \frac{H}{|t|^{\beta+\delta}}$, the scaling equation of state can be written as:

$$m = f_{\pm}(h) \tag{6}$$

Equation (6) implies that for the true scaling relations and the right choice of β, γ, and δ values, scaled m plotted as a function of scaled h will fall on two universal curves: one above T_c and another below T_c. In order to check if these critical exponents can generate the scaling equation of state Eq. (6) for $Gd_{60}Co_{40-x}Mn_x$, the scaled m versus scaled h is plotted in Fig. 4 taking critical exponents from Table I. It is rather significant that all the data collapse into two separate branches: one below T_c and another above T_c. This clearly indicates that the obtained critical exponents are reliable, and the interactions get properly renormalized in critical regime following scaling equation of state. Similar behavior has also been found for the whole series of alloys studied in this work.

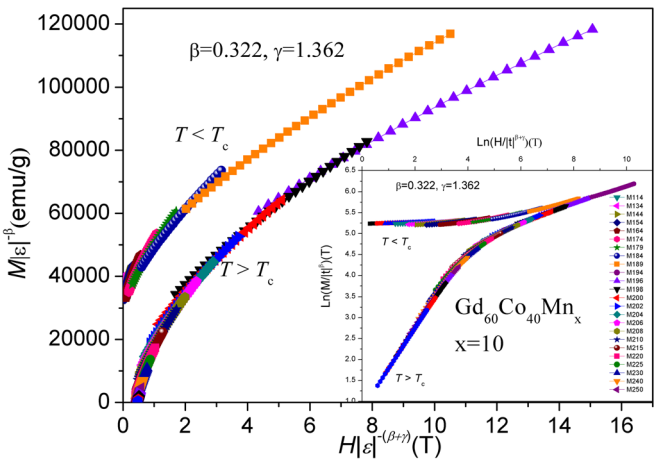

FIG. 4. (Color online) The scaled m are plotted as a function of scaled h for $Gd_{60}Co_{40-x}Mn_x$ (x = 10) alloy. The plot shows all the data collapse into two distinct branches: one below T_c and another above T_c. Inset shows the same plot on log−log scale.

The Curie temperature of amorphous $Gd_{60}Co_{40-x}Mn_x$ (x = 0, 5, 10, 15) alloys can be tuned from 198 K to 205 K with increasing Mn content. The maximum values of $-\Delta S_M$ are 7.7, 7.1, 6.2 and 5.4 $J \cdot kg^{-1} \cdot K^{-1}$ for $Gd_{60}Co_{40-x}Mn_x$ with x = 0, 5, 10, and 15, respectively, under the applied field change from 0 to 5 T. The $Gd_{60}Co_{40-x}Mn_x$ amorphous alloys exhibit second order magnetic phase transition from FM to PM state. The values of critical exponents for describing the FM to PM second order transition are extracted using KF method and field dependence of MCE. The critical exponent values obtained for all samples are comparable to the values predicted by the 3D Ising model, and have also been verified by the scaling equation of state.

This work is supported by Guangdong Provincial Science and Technology Program (Grant No. 2010B050300008), the Fundamental Research Funds for the Central Universities, SCUT (Grant Nos. 2012ZZ0013 and 2011ZM0014), China Postdoctoral Science Foundation (20110490875). V. F. acknowledges the financial support of the Spanish Ministry of Science and Innovation and EU FEDER (Project MAT 2010-20537), the PAI of the Regional Government of Andalucía (Project FQM-6462), and the United States Office of Naval Research (Project N00014-11-1-0311).

[1]H. Fu, X. T. Zu, and T. D. Shen, Thermochim. Acta **445**, 53 (2006).
[2]Z. Lin, S. Li, S. Tsai, J. Duh, M. Liu, and F. Xu, J. Magn. Magn. Mater. **323**, 1741 (2011).
[3]M. Zou, J. A. Sampaio, V. K. Pecharsky, and K. A. Gschneidner, Phys. Rev. B **80**, 172403 (2009).
[4]L. G. de Medeiros, Jr., N. A. de Oliveira, and A. Troper, J. Magn. Magn. Mater., **322**, 1558 (2010).
[5]M. Hudl, P. Nordblad, T. Björkman, O. Eriksson, L. Häggström, M. Sahlberg, Y. Andersson, E. K. Delczeg-Czirjak, and L. Vitos, Phys. Rev. B, **83**, 134420 (2011).
[6]V. K. Sharma, M. K. Chattopadhyay, L. S. S. Chandra, and S. B. Roy, J. Phys. D Appl. Phys., **44**, 145002 (2011).
[7]R. Caballero-Flores, V. Franco, A. Conde, K. E. Knipling, and M. A. Willard, Appl. Phys. Lett. **96**, 182506 (2010).
[8]Q. Y. Dong, B. G. Shen, J. Chen, J. Shen, H. W. Zhang, and J. R. Sun, J. Appl. Phys., **105**, 07A305 (2009).
[9]X. C. Zhong, P. F. Tang, Z. W. Liu, D. C. Zeng, Z. G. Zheng, H. Y. Yu, W. Q. Qiu, and M. Zou, J. Alloy. Compd. **509**, 6889 (2011).
[10]C. L. Zhang, D. H. Wang, Z. D. Han, H. C. Xuan, B. X. Gu, and Y. W. Du, J. Appl. Phys. **105**, 013912 (2009).
[11]H. Fu, M. S. Guo, H. J. Yu, and X. T. Zu, J. Magn. Magn. Mater. **321**, 3342 (2009).
[12]Y. K. Fang, C. H. Lai, C. C. Hsieh, X. G. Zhao, H. W. Chang, W. C. Chang, and W. Li, J. Appl. Phys. **107**, 09A901 (2010).
[13]S. Gorsse, B. Chevalier, and G. Orveillon, Appl. Phys. Lett. **92**, 122501 (2008).
[14]Z. G. Zheng, X. C. Zhong, K. P. Su, H. Y. Yu, Z. W. Liu, and D. C. Zeng, Sci. China, Ser. G **54**, 1 (2011).
[15]J. Y. Fan, L. S. Ling, B. Hong, L. Zhang, L. Pi, and Y. H. Zhang, Phys. Rev. B **81**, 144426 (2010).
[16]S. N. Kaul, J. Magn. Magn. Mater. **53**, 5 (1985).
[17]V. Franco, A. Conde, V. Provenzano, and R. D. Shull, J. Magn. Magn. Mater. **322**, 218 (2010).
[18]V. Franco and A. Conde, Int. J. Refrig. **93**, 465 (2010).
[19]M. Halder, S. M. Yusuf, M. D. Mukadam, and K. Shashikala, Phys. Rev. B **81**, 174402 (2010).
[20]A. K. Pramanik and A. Banerjee, Phys. Rev. B **79**, 214426 (2009).
[21]P. M. Shand, J. G. Bohnet, N. H. Jensen, J. Goertzen, V. J. Litwinowicz, J. E. Shield, D. C. Schmitter, G. Rojas, and D. L. Leslie-Pelecky, J. Magn. Magn. Mater. **322**, 3303 (2010).
[22]P. M. Shand, J. G. Bohnet, J. Goertzen, J. E. Shield, D. Schmitter, G. Shelburne, and D. L. Leslie-Pelecky, Phys. Rev. B **77**, 184415 (2008).